Author Manuscript

Author Manuscript

Author Manuscript

Author Manuscript

HHS Public Access

Author manuscript

Cancer Res. Author manuscript; available in PMC 2017 April 01.

Published in final edited form as:

Cancer Res. 2016 October 1; 76(19): 5870–5880. doi:10.1158/0008-5472.CAN-15-3196.

An integrated nanotechnology-enabled transbronchial image-guided intervention strategy for peripheral lung cancer

Cheng S. Jin[1,2,3,*], **Hironobu Wada**[4,*], **Takashi Anayama**[4], **Patrick Z McVeigh**[5], **Hsin Pei Hu**[4], **Kentaro Hirohashi**[4], **Takahiro Nakajima**[4], **Tatsuya Kato**[4], **Shaf Keshavjee**[4], **David Hwang**[6], **Brian C. Wilson**[3,5], **Gang Zheng**[1,2,3,5,#], and **Kazuhiro Yasufuku**[3,4,#]

[1]Graduate Department of Pharmaceutical Sciences, Leslie Dan Faculty of Pharmacy, University of Toronto, Canada, M5S 3M2

[2]Institute of Biomaterial and Biomedical Engineering, University of Toronto, Canada, M5S 3G9

[3]Princess Margaret Cancer Centre and TECHNA Institute, University Health Network, Canada, M5G 1L7

[4]Division of Thoracic Surgery, Toronto General Hospital, University Health Network, Canada, M5G 2C4

[5]Department of Medical Biophysics, University of Toronto, Canada, M5S 1L7

[6]Division of Experimental Therapeutics, Respiratory & Critical Care, Princess Margaret Cancer Centre, Canada, M5G 2C4

Abstract

Early detection and efficient treatment modality of early-stage peripheral lung cancer is essential. Current non-surgical treatments for peripheral lung cancer show critical limitations associated with various complications, requiring alternative minimally invasive therapeutics. Porphysome nanoparticle-enabled fluorescence-guided transbronchial photothermal therapy (PTT) of peripheral lung cancer was developed and demonstrated in preclinical animal models. Systemically-administered porphysomes accumulated in lung tumors with significantly enhanced disease-to-normal tissue contrast, as confirmed in three subtypes of orthotopic human lung cancer xenografts (A549, H460 and H520) in mice and in an orthotopic VX2 tumor in rabbits. An in-house prototype fluorescence bronchoscope demonstrated the capability of porphysomes for *in vivo* imaging of lung tumors in the mucosal/submucosal layers, providing real-time fluorescence guidance for transbronchial PTT. Porphysomes also enhanced the efficacy of transbronchial PTT significantly and resulted in selective and efficient tumor tissue ablation in the rabbit model. A clinically used cylindrical diffuser fiber successfully achieved tumor-specific thermal ablation, showing promising evidence for the clinical translation of this novel platform to impact upon non-surgical treatment of early-stage peripheral lung cancer.

[#]**Corresponding authors:** Dr. Gang Zheng, Tel: 1-416-581-7666, gzheng@uhnres.utoronto.ca, Princess Margaret Cancer Centre, 101 College Street, TMDT 5-354, Toronto, Ontario, Canada, M5G 1L7. Dr. Kazuhiro Yasufuku, Tel: 1-416-581-7486, Kazuhiro.Yasufuku@uhn.ca, Division of Thoracic Surgery, Toronto General Hospital, University Health Network. 200 Elizabeth Street, 9N-957, Toronto, ON, Canada, M5G 2C4.

[*]co-first authors

Conflict of interest: no conflicts to disclose.

Author Manuscript Author Manuscript Author Manuscript Author Manuscript

Keywords

Lung cancer; Image-guided; Photothermal therapy; Porphyrin; Nanotechnology

Introduction

Despite remarkable advances in technology and treatment options, lung cancer remains the leading cause of cancer mortality in the Western world. Early detection is the key for achieving survival benefit, which has led to increasing demand for treatment of early-stage lung cancer (1). Anatomical resection is the standard of care for early-stage disease; however certain patients may be precluded due to significant co-morbidities. Non-surgical therapeutics are current alternatives, including stereotactic body radiation therapy (SBRT) (2-9), CT-guided percutaneous radiofrequency ablation (10-14) and bronchoscopic laser therapy (15, 16). New techniques such as CT-guided percutaneous microwave (17) and cryoablation (18) are under investigation as well. However, limitations still exist for each modality. SBRT may have serious radiation toxicity, such as pneumonitis, which restricts repeat irradiation in the primary radiation field, while CT-guided RFA can cause pneumothorax and pleural effusion with a high reported frequency of up to 20% (13, 14). In addition, RFA excludes tumors adjacent to major vessels due to high risk of lethal bleeding caused by non-selective ablation. Drawbacks of CT-guided percutaneous approach also include excessive radiation dose and poor access due to the overlying scapula. Furthermore, the treatment outcome of CT-guided RFA, microwave and cryoablation depends critically on the placement of the treatment probe, resulting in low efficiency and low tumor specificity. Similarly, bronchoscopic high-power laser therapy is confined to direct ablation of centrally-located tumors, as its poor selectivity requires the ablation to be monitored and controlled in real-time (15). By contrast, bronchoscopic photodynamic therapy (PDT) has the advantage of good tumor-specific tissue destruction and minimal side effects, because of tumor-preferential accumulation of PDT photosensitizers combined with localized laser irradiation. However, the indications for PDT are limited to centrally-located lesions, while CT-guided percutaneous PDT for peripheral lesions is still investigational (19). Further limitations include its oxygen-dependent mechanism of action, leading to reduced efficacy in hypoxic tumors (20, 21). Hence, oxygen-independent photothermal therapy (PTT) (22) delivered by a transbronchial approach with real-time visual guidance could be a novel alternative. Similar to PDT, systemically-administered photothermal enhancers can contribute markedly to tumor-specific ablation with local laser treatment: upon near-infrared laser irradiation, PTT agents efficiently absorb light and dissipate the absorbed energy through heating, resulting in irreversible cell damage (23, 24).

We have recently described multi-modal ‘porphysome’ nanoparticles self-assembled from phospholipid-porphyrin conjugates and have a liposome-like bilayer structure (25). Porphysomes accumulate in cancer with tumor-to-muscle concentration ratios typically ≥ 10:1 in subcutaneous tumors (26), attributed to the enhanced permeability and retention (EPR) effect (27, 28). The highly packed porphyrin-lipids in the porphysome bilayer (>80,000 per particle) absorb light with an extinction coefficient of 10^8-10^{10} $M^{-1}cm^{-1}$ that is comparable to metal nanoparticles and convert the light energy to heat with extremely high

Author Manuscript Author Manuscript Author Manuscript Author Manuscript

efficiency. Porphysomes have been shown to enhance the photothermal effect significantly, eradicating mouse subcutaneous tumor models with no recurrence (25, 29). Although the fluorescence of intact porphysomes is highly quenched, the small fraction of porphysomes dissociated locally in the tumor interstitium and exhibited sufficient fluorescence intensity for image detection (25), so that porphysomes have the capability of both tumor fluorescence detection and tumor-selective PTT, demonstrated in both mice with subcutaneous tumor model and orthotopic rabbit head and neck cancer model (25, 30).

The objective of this study was to establish a minimally-invasive transbronchial PTT platform for bronchoscopic image-guided treatment of early-stage peripheral lung cancer, integrating clinically-relevant *in vivo* tumor models, the multi-modal porphysome nanoparticles, a prototype fluorescence bronchoscope and transbronchial optical laser irradiation. First, the porphysome biodistribution was examined in orthotopic human lung cancer xenografts (adenocarcinoma A549, large cell carcinoma H460, and squamous cell carcinoma H520) in nude mice, and in a VX2 tumor in the rabbit lung as a larger model in which to test a prototype fluorescence bronchoscope for fluorescence image-guided porphysome-enhanced transbronchial PTT. This study provides fundamental support for translation of this novel platform into patients as a minimally invasive treatment for lung cancer (Figure 1).

Materials and Methods

All animals received humane care in accordance with the policies formulated by the institutional Animal Care Committee (University Health Network, Toronto), the Animal for Research Act of the Province of Ontario and the Canadian Council on Animal Care. All animal studies were approved by the UHN Animal Care Committee.

Formation of porphysomes

Porphysomes were synthesized following a protocol reported previously (29). The lipid film of porphysomes consists of 55 mol % porphyrin-lipid (pyropheophorbide-lipid), 40 mol % cholesterol (Avanti Polar Lipids, Alabaster, AL, USA) and 5 mol % distearoyl-sn-glycero-3-phosphoethanolamine-N-methoxy(polyetheneglycol) (PEG2000-DSPE, Avanti). Lipid films were dried under a gentle stream of nitrogen gas, followed by 1 h under vacuum. Each lipid film was then rehydrated with PBS buffer (150 mM, pH 7.5) at a concentration of 10 mg/mL and extruded through a polycarbonate membrane (pore size = 100 nm) 10 times. The porphyrin concentration was determined by UV/Vis spectroscopy (Varian Inc., Palo Alto, CA, USA). Porphysomes were kept sterile and stored at 4 °C prior to use.

Animal models

Nude mouse orthotopic lung cancer models and VX2 tumor grown in rabbit lung were used. A suspension of cancer cells (7×10^5 cells in 70 μL) was inoculated into the peripheral airway of nude mice (NCr-Foxn1nu; Taconic Farms Inc, Hudson, NY, USA) by a non-invasive, surgical microscopy-guided, trans-oral inoculation technique: this does not require skin incision and avoids non-specific porphysome accumulation due to wound inflammation (31). Three different human lung cancer models were used: A549 adenocarcinoma, H520

Author Manuscript Author Manuscript Author Manuscript Author Manuscript

squamous cell carcinoma and H460 large cell carcinoma. The tumor model in the rabbit (New Zealand White; Charles River, Saint Constant, QC, Canada) was created by transbronchial inoculation with VX2 tumor cells into the lung parenchyma using an ultra-thin bronchoscope (BF type XP160F, Olympus Medical Systems Corp., Tokyo, Japan) through a miniature laryngeal mask (32).

Porphysome accumulation in mouse and rabbit tumor models

The *in vivo* biodistribution and pharmacokinetics of porphysomes were assessed in the mouse (n=5) and rabbit (n=4) models. After confirming tumor by micro-CT scanning, 20 mg/kg of porphysomes (total lipid) was administrated intravenously to animals. At 48 h post-injection, the animals were euthanized by sodium pentobarbital (Bimeda-MTC Animal Health Inc. Cambridge, ON, Canada) and organs of interest were harvested. Porphysome accumulation in normal lung and orthotopic lung tumor was first visualized by *ex vivo* fluorescence system (Maestro EX 2.10, Cambridge Research & Instrumentation, Inc., Waltham, MA, USA) with 575-605 nm excitation and >645 nm detection using 500 ms integration time. To further compare the porphysome accumulation in tumor and normal lung, tissues were frozen in OCT gel, sectioned (5 μm) and stained with nuclei-staining DAPI. The frozen slides were imaged by confocal microscopy using a 60× oil-immersion lens (633 nm excitation for porphyrin and 408 nm excitation for DAPI). For the biodistribution analysis, organs of interest were freshly weighed and homogenized in PBS, the porphyrin fluorescence in the supernatant was measured by spectrofluorimetry and the percent of injected dose per gram (ID%g) of tissue was calculated based on a standard porphyrin-lipid concentration curve.

Porphysome-enhanced ex vivo PTT of VX2 tumor in rabbit lung

At 48 h post-injection of 20 mg/kg porphysomes, rabbits were sacrificed and the tumor was dissected for *ex vivo* PTT. The tumor was cut into 5 mm cubes and irradiated for 1 min (straight-cut fiber, 671 nm, 6 mm irradiation diameter). Laser powers of 250, 500 and 750 mW were compared, giving the light intensity of 0.88 W/cm^2, 1.77 W/cm^2, and 2.65 W/cm^2, respectively. Tumor from uninjected rabbits was used as the control. The tumor temperature was monitored using a near-infrared thermal camera once every 10s during irradiation and for 1 min after irradiation. n=3 was used in each group for average and S.D. values.

Porphysome fluorescence bronchoscopy

We have developed a novel ultrathin flexible endoscope system in collaboration with Olympus Medical Systems Corp, Japan to visualize the red/near-infrared fluorescence of the porphysomes dissociated locally in the tumor. To maximize the fluorescence signal, a red diode source (650-670 nm) was added to the white light source. The flexible ultrathin fiber bronchoscope (BF type XP60) was connected to an optical filter unit in which the porphysome fluorescence was separated by a 678 nm long-pass filter. White-light and fluorescence images were captured individually by separate CCD cameras and displaced side-by-side on the same monitor (Figure 4A). The *in vivo* porphysome fluorescence was visualized in the rabbit model: after standard white-light examination, fluorescent bronchoscopic imaging was carried out immediately prior to and then at 24 and 48 h after IV

Author Manuscript Author Manuscript Author Manuscript Author Manuscript

injection of 20 mg/kg porphysomes. Repeated bronchoscopic examination was enabled using minimally-invasive airways management with a miniature laryngeal mask (32).

Porphysome-containing tissue-mimicking phantoms

The porphysome-enhanced photothermal effect was validated first using porphysome-containing optically transparent phantoms that mimic thermal protein coagulation for visualizing the thermal lesions (33). Porphysome nanoparticles were added into the phantom gel formulation at three concentrations: 0, 29 and 58 nM, which were calculated based on the *in vivo* biodistribution in the rabbit VX2 tumor at 48 h post-injection (0.16% ID/g ≅ 58 nM).

Photothermal dosimetry for optimization of laser ablation

A straight-cut type fiber (Figure 5A-a, 200 μm in core diameter, Laserglow Technologies, Toronto, ON, Canada) and a cylindrical diffuse fiber (Figure 6A-b, 1.65 mm in tip outer diameter, OPTIGUIDE® DCYL 225, AngioDynamics, Queensbury, NY, USA), were used for *in vivo* PTT of VX2 tumor in the rabbit lung. A dosimetry study was carried out first to optimize the laser power by inserting the fiber into the porphysome-containing phantoms, as shown in Figure 5A and Figure 6A, and the temperature rise was monitored using a near-infrared thermal camera (Mikroshot®, LUMASENSE Technologies, Santa Clara, CA, USA) once per min during the 10 min 671 nm diode laser irradiation at either 250 mW for the straight-cut fiber or 500 mW/cm for the diffuser fiber. Experiments were done in triplicate.

Transbronchial photothermal ablation

The rabbit lung VX2 tumor model was used to validate porphysome-enhanced transbronchial photothermal ablation. The responses were comprehensively assessed for both tumor destruction and collateral damage to adjacent normal tissues. After inserting a miniature laryngeal mask for general anesthesia, white-light bronchoscopic inspection was used to localize the tumor, with or without the assistance of fluorescence imaging and X-ray fluoroscopy. Thereafter, the straight-cut type fiber was loaded into a bronchoscopic aspiration needle (MAJ-65, Olympus) and placed through the accessory channel of the bronchoscope. The needle was inserted into the center of the tumor and the fiber was introduced into the tumor. The tumor was then irradiated at 250 mW for 10 min to achieve a lethal temperature of ≥55 °C throughout the tumor mass (34). 8 rabbits with porphysomes injection (20mg/kg of total lipid) at 48 h prior to laser irradiation and 4 rabbits without injection were treated by laser to evaluate the therapeutic efficacy of porphysome-enhanced PTT.

Transpleural photothermal ablation using diffuser laser fiber

Surgeons exposed the rabbit lung containing the orthotopic VX2 tumor, and the lung was inflated and manually ventilated. Porphysome fluorescence in the tumor was imaged by the fluorescence endoscope (Figure 4A). The tumor was stabilized by palpation and then an 18G needle was inserted through it as a channel to place the laser fiber into the center of the tumor and irradiated for 10 min. The lung was inflated and manually ventilated during the

Author Manuscript Author Manuscript Author Manuscript Author Manuscript

irradiation, mimicking the conditions of transbronchial ablation. Ablation of normal peripheral lung was performed in the same way.

Histopathological evaluation of the photothermal effect

Immediately post-ablation, the animals were sacrificed by IV injection of sodium pentobarbital and the entire lung with the treated tumor was removed, fixed in Tissue-Tek OCT and stored at -80°C for frozen tissue sectioning to evaluate both morphological changes (H&E staining) and cell viability using nicotinamide adenine dinucleotide-diaphorase (NADH) enzyme-activity staining (35). Since the lack of NADH staining indicates no cell viability, the ablated volume was estimated by the following formula;

$$V=\frac{4}{3}\pi\,(\text{long radius})\,(\text{short radius})^2 \quad (36)$$

The long and short radii were measured from the non NADH-stained area, with tumor vs. normal lung tissue delineated by the gross section and H&E staining. Since the ablated volume by the diffuser type fiber should be proportional to the fiber length in the target tumor, the above formula is not exact but allows a straight-forward comparison of the results for the different conditions.

Statistical analysis

Graphs were created and statistics were calculated by GraphPad Prism software (version 5.01, La Jolla, CA), and presented as means and S.D.. The two-tailed Student's t test was used to compare two groups. To compare the efficacy of porphysome-enabled PTT among multiple groups, one-way analysis of variance (ANOVA) with Tukey's multiple comparison test were used for the comparisons of three or four variables. All p-values were based on a two-sided hypothesis, with $p < 0.05$ considered significant.

Results

Porphysome accumulation in nude mice orthotopic human lung cancer xenografts

PTT agents with selective tumor accumulation contribute to enhanced tumor-specific photothermal ablation. The biodistribution of porphysomes was compared between 24 and 48 h post intravenous injection in the nude mouse A549 orthotopic lung cancer model. At both time points, the porphysome fluorescence was clearly visible in the tumor *ex vivo*, both using a imager (Figure 2A, B; Supplementary Figure S1A, B) and confocal microscopy (Figure 2C; Supplementary Figure S1C), while much weaker fluorescence was observed in the normal lung parenchyma (Supplementary Figure S1B): the average concentration in the tumor tissue was 1.29 ± 0.52% ID/g, representing a 2.70 ± 0.96 fold increase over the concentration of 0.51 ± 0.15 %ID/g in normal lung (Supplementary Figure S1D). At 48 h the accumulation in both tumor and lung decreased to 0.85 ± 0.18% and 0.25 ± 0.13% ID/g, respectively, but the tumor-to-lung ratio increased to 3.67 ± 1.14 (Figure 2D). The other two human lung cancer xenografts (large cell carcinoma H460 and squamous cell carcinoma H520) were subsequently tested at 48 h post-injection and marked fluorescence was observed (Figure 2A,C), with accumulations in H460 and H520 of 1.16 ± 0.28% and 0.90 ± 0.1%ID/g, respectively, corresponding to tumor-to-lung ratios of 4.0 ± 1.59 and 5.16

Author Manuscript Author Manuscript Author Manuscript Author Manuscript

± 1.51 (Figure 2D). The uptake of porphysomes in other tissues at 24 h post-injection is shown in Supplementary Figure S2.

Porphysome accumulation in VX2 tumor and porphysome-enhanced PTT in rabbit

Using the 48 h time point, fluorescence imaging *ex vivo* was repeated in the VX2 tumor model grown in the rabbit lung. The tumors were clearly identified by their strong fluorescence (white circle in Figure 3A). The porphysome biodistribution (Figure 3B) demonstrated accumulation in tumor of 0.16 ± 0.07% ID/g, which was 2.1 ± 1.0 times that in normal lung (0.076 ± 0.02% ID/g).

Since the porphysomes start to disassemble into their porphyrin-lipid components and their fluorescence becomes unquenched upon accumulation in tissue, there is an optimal time point between having adequate fluorescence for *in vivo* imaging and high enough concentration of intact nanoparticles for efficient photothermal enhancement. Since the concentration of remaining intact porphysomes in the tumor at 48 h post-injection could not be measured quantitatively, we conducted laser irradiation on *ex vivo* tumors harvested at 48 h post-injection to evaluate the enhanced heat generation. During the 1 min irradiation with 671 nm light, the average tumor temperature increased by 6.3 ± 1.5, 17.5 ± 3.5 and 34.7 ± 3.8°C for incident laser powers of 250, 500 and 750 mW, respectively, while the corresponding temperature increases in control uninjected tumors were only 1.3 ± 1.6, 5.4 ± 1.8 and 10.9 ± 2.6 °C (Figure 3C). This result indicates that there is adequate concentration of intact porphysomes in the tumor at 48 h post-injection to give marked PTT enhancement.

Porphysome-enabled fluorescence bronchoscopic detection of VX2 tumor in rabbit lung

The set-up of prototype fluorescence bronchoscopic system was demonstrated (Figure 4A). In an example case in the rabbit model, CT scanning (Figure 4B) showed tumor adjacent to the right lower bronchus but not extending to the bronchial mucosal surface, so it was invisible on neither white light nor fluorescence bronchoscopy before the injection of porphysomes (Figure 4D-a and b). At 24 h post-injection, bright fluorescence could be seen over the whole imaging field of the bronchoscope (Figure 4D-c), and the contrast between tumor and adjacent normal lung tissue was enhanced at 48 h post-injection when fluorescence of the normal bronchial wall had washed out (Figure 4D-d), leaving the clearer fluorescent delineation of tumor than 24 h within the tumor. Shown in the Supplementary Video S1 taken at 48 h post-injection, bright fluorescence signal was observed while the bronchoscope channel was being moved along the bronchus into the peripheral area of lung (starting from 10^{th} second of Supplementary Video S1), indicating the existing porphysome-containing lung tumor beneath the bronchial mucosal surface. In Supplementary Video S2, the signal observed by fluorescence bronchoscopy was highlighted as green, demonstrating the location of porphysome-containing lung tumor more precisely. Histopathology subsequently confirmed that the tumor was confined to the sub-mucosal layer without extending to the endobronchial lumen (Figure 4C), demonstrating that subsurface tumor which is easily missed by white-light bronchoscopy can be successfully visualized and detected by its porphysome fluorescence using this bronchoscopy system. Since the 48 h time point fulfills both the needs of fluorescence tumor identification and efficient

Author Manuscript Author Manuscript Author Manuscript Author Manuscript

photothermal enhancement, it was chosen for the following *in vivo* fluorescence-guided PTT studies.

Photothermal dosimetry using porphysome-containing tissue-mimicking phantoms

To evaluate the photothermal efficacy of porphysomes to destroy lung tumor *in situ*, a straight-cut (cleaved) optical fiber was used, since this is small enough (200 μm diameter) to fit into a 21G needle placed within the ultra-thin bronchoscope accessory channel for transbronchial therapeutic light delivery. Before conducting *in vivo* PTT, the efficacy of this light delivery was evaluated in porphysome-containing phantoms (Figure 5A and B). A maximum temperature of 55°C *in vivo* is commonly targeted to achieve tissue destruction (34), so an 18°C temperature increase from baseline was used as the target threshold. Since the porphysomes in the phantom are still intact, their fluorescence was minimal (Supplementary Figure S3), and the heat generation observed in this phantom study revealed the true PTT property of porphysomes. During the 10 min irradiation (671 nm, 250 mW), the maximum temperature increase was 14.6 ± 2.5°C in the phantom containing 29 nM porphysomes (= 0.076% ID/g in the rabbit lung cancer model) and 21.2 ± 3.5 °C at 58 nM concentration (= 0.16% ID/g) (Figure 5C-a). Notably, the axial distance of the ≥18 °C temperature increase was only around 3 mm from the laser fiber in the 58 nM phantom (Figure 5C-b).

Transbronchial PTT of peripheral lung tumor with straight-cut fiber

We evaluated the effectiveness of porphysome-enhanced transbronchial PTT in the *in vivo* rabbit model and the detailed results are presented in Supplementary Table 1. A delivered light power of 250 mW was selected initially to minimize unexpected damage to normal tissue. Of 8 rabbits with porphysome injection, 3 showed accurate tumor ablation, while the remaining 5 showed ablation of adjacent lung parenchyma, not of the tumor. Similarly, in the 4 control uninjected rabbits the laser fiber was always inserted into lung parenchyma instead of tumor; therefore, no damage was detected in the uninjected tumor, but regions of lung parenchyma were ablated. The ablated area in each rabbit was identified on the NADH-stained slides and the morphological changes were further confirmed on the H&E stained slides (Supplementary Figure S4). The cells in the ablated area showed evidence of thermal artifact, including deeply eosinophilic-staining cytoplasm and hyperchromatic nuclei, with loss of nuclear detail in H&E-stained sections. The estimated PTT-ablated volume showed significant differences between these three groups by one-way ANOVA (p=0.001). When comparing two groups, significantly larger ablation was observed in the group of porphysome-containing tumor (27.0 ± 10.4 mm^3) than the porphysome-containing normal lung (6.8 ± 3.6 mm^3, p=0.004 by t-test) and the control uninjected lung (6.6 ± 4.8 mm^3, p=0.01 by t-test), demonstrating successful porphysome-enhanced PTT (Figure 5D, E).

Transpleural photothermal ablation of peripheral lung tumor with increased laser output

Aiming at achieving larger ablated volumes of tumor within the same irradiation time, an increased laser output of 500 mW was tested (n=5). We first evaluated the heat generation using porphysome-containing phantoms. Increasing the optical power to 500 mW increased the temperature of the 29 nM and 58 nM phantoms to 36.5 ± 6.7 and 63.6 ± 10.2°C, respectively, and resulted in greater ablated areas (>9 mm axial distance Supplementary

Author Manuscript Author Manuscript Author Manuscript Author Manuscript

Figure S5A). In this cohort of rabbits, a transpleural approach after thoracotomy was used instead of the transbronchial approach because the optical fiber could be inserted into the tumor more accurately under direct palpation compared to brochoscopic laser fiber insertion (Note: that this is not possible in patients.) This resulted in an ablation volume of 116 and 141 mm^3 in two rabbits (average value 128 mm^3), i.e. 5-fold greater than at 250 mW (Supplementary Figure S5B); however, the temperature of the fiber tip reached 70°C, resulting in thermal damage to the tissue without porphysomes: 40.1 and 27.8 mm^3 in tumors of two rabbits (average 33.9 mm^3) and 26.9 mm^3 in normal lung with n=1.

Transpleural photothermal ablation of peripheral lung tumor with diffuser fiber

To take the advantage of higher laser power while avoiding the self-heating problem, a commercial fiber with a 2.5 cm cylindrical diffuser tip was used (tip outer diameter: 1.65 mm). A dosimetry study was first carried out and the temperature change was determined along the radial distance from the fiber. The fiber tip was at 33°C at a power density of 500 mW/cm, and slightly increased the temperature in the phantom by 6.4 ± 3.6 °C from room temperature (Figure 6A). The corresponding maximum temperature increases in the 29 nM and 58 nM porphysome-containing phantoms were 16.6 ± 1.5 and 18.1 ± 0.4°C, respectively (Figure 6B). A cylindrical volume of 6 mm diameter reached the threshold temperature increase of ≥18 °C. Since the fiber tip did not fit into the bronchoscopic needle, PTT was conducted with transpleural irradiation. After thoracotomy, distinct fluorescence localized the tumor (Figure 6C), while no significant fluorescence was detected in control tumors without porphysomes. In this cohort of rabbits, 4 groups were prepared: porphysome-containing tumors (n=3), porphysome-containing normal lung (n=4), control (no porphysome) tumor (n=4), and control lung (n=3). The cells were considered as thermally killed based on deep eosinophilic-staining cytoplasm and hyperchromatic nuclei with loss of nuclear detail (Supplementary Figure S6). The ablated area was identified based on the NADH staining, and one-way ANOVA indicated the significant difference between these four groups ($p<0.0001$). The porphysome-containing tumor showed the largest ablated volume (76.3 ± 13.2 mm^3) among all groups, this being 4.4 times greater than in porphysome-containing normal lung (17.3 ± 6.7mm^3, and p=0.0005 by t-test) (Figure 6D, E). Furthermore, there was minimal damage in non-porphysome tissues, either tumor (0.1 ± 0.08 mm^3) or normal lung (1.3 ± 1.9 mm^3), with p<0.001 by t-test when comparing to porphysome-containing tumor.

Discussion

Successful focal therapy provides complete tumor destruction with minimal damage to adjacent tissues, which requires the synergistic optimization of precise target tumor delineation, accurate ablative energy delivery and preservation of healthy tissue. The unique structure and physiochemical properties of porphysome nanoparticles combined with red or near-infrared laser irradiation achieved significantly larger ablation than the laser alone delivered by transbronchial endoscope, showing the promising potential to treat early-stage lung cancer with high specificity. The minimally-invasive, porphysome-enabled, fluorescence-guided, transbronchial PTT approach shown here has been optimized and validated using clinically-relevant available animal models: the orthotopic xenograft model

Author Manuscript Author Manuscript Author Manuscript Author Manuscript

in mice demonstrates that the PTT treatment can ablate human lung tumor tissue, while the VX2 model, although not itself a lung tumor, shows the ability to selectively destroy tumor tissue in the setting of the lung.

The nanostructure of porphysomes converted monomeric porphyrins from PDT to PTT mechanism, offering the advantage over PDT (such as photofrin-enabled PDT) in treating the hypoxia existing in tumor or induced by phototherapy (22). Besides, the stable nanostructure likely contributes to their prolonged circulation time and preferential tumor accumulation after IV administration. We previously reported that porphysomes accumulate in subcutaneous tumors and orthotopic prostate tumors preferentially via the EPR effect due to their ~100 nm size (22, 25, 37). In the present study, consistent accumulation was confirmed in all three human lung cancer xenografts and in the VX2 tumor, with marked tumor-to-lung contrast at 48 h post-injection. Compared to indocyanine green (ICG) topically injected surrounding tumor for PTT (38), porphysome achieved highly tumor-specific and efficient PTT by its tumor-preferential accumulation and high extinction coefficient (porphysome:10^8-10^{10} $M^{-1}cm^{-1}$ at 671 nm vs ICG: 2.42×10^4 $M^{-1}cm^{-1}$at 830 nm) (39). Together with the targeted light placement, this tumor-selective porphysome accumulation provides a new element of control in PTT to improve efficacy and safety.

In addition, porphysomes are intrinsically capable of fluorescence imaging because of the porphyrin-lipid composition. This facilitated the localization of tumor (Supplementary Videos 1 and 2), revealing the potential application of fluorescence-guided transbronchial PTT. For comparison, in the rabbits without porphysome-injection the laser fiber was misplaced into normal lung parenchyma in all cases, showing that standard white-light bronchoscopy does not provide adequate tumor delineation. However, the fluorescence guidance was only successful for the tumor close to the bronchial wall, due to the limited penetration depth of porphyrin fluorescence. Therefore, the depth of tumor from bronchial wall should be taken into consideration in patients for accurate ablation, and CT scanning can aid treatment planning to select proper patients for transbronchial PTT.

The natural physiological structure of the lung also helped to reduce the heat damage to normal tissue. The air-containing lung parenchyma and large pulmonary vessels both reduce heat spreading from the target tumor during irradiation (40-42). The resulting thermal damage in lung parenchyma was significantly less than the ablated tumor volume in the rabbit model (Figure 5D, Figure 6D). However, the temperature at the tumor boundary might not reach the required thermal damage threshold (~55°C), resulting in incomplete ablation and risk of tumor recurrence. Hence, it may be beneficial to monitor the temperature during treatment, for example by MR-thermometry that has been used clinically in other focal therapies, such as PTT of prostate cancer (43).

In terms of optimizing the light delivery, comprehensive *in vivo* studies were conducted to explore the translational potential of porphysome-enhanced focal PTT to treat lung cancer. First, we have shown that the use of a simple straight-cut (cleaved) fiber did achieve enhanced PTT ablation with the injection of porphysomes, but did not provide the required ablation volume without normal tissue damage. The use of a commercially-available cylindrical diffuser fiber, which is currently employed widely in clinical photodynamic

Author Manuscript Author Manuscript Author Manuscript Author Manuscript

therapy for both endoscopic and interstitial light delivery (44), overcame the limitation. However, the cynlindrical diffuser fiber is currently too large to pass through the ultrathin bronchoscope channel (which is why we performed the rabbit studies transpleurally) and required additional needles to penetrate through the bronchial wall for insertion due to the blunt tip of the fibers. Hence, for clinical translation, much thinner diffuser fibers will be required, such as those reported based on fiber Bragg gratings (44), and an integrated sharp tip or other introducer device is needed. Additionally, the light intensity decreased rapidly from laser fiber due to the high extinction coefficient of porphysome. The current cylindrical diffuser fiber has the light intensity limit at 500 mW/cm, so the increase of the laser output with higher light intensity will ablate larger area. One can also envisage multiple placement of laser fiber to achieve full coverage in disease following the protocol in clinical prostate cancer treatment (43). Therefore, with the further development of fiber placement protocol, minimally-invasive transbronchial PTT can be expanded into first clinical trials.

The unique structure and physiochemical properties of porphysomes also enable other imaging and therapeutic options. Porphysomes can be labeled with radioisotopes such as ^{64}Cu for PET imaging (45, 46) or with Mn for MRI contrast (47), enabling tumor delineation for treatment planning. The latter may also enhance the photostability of porphysomes. Furthermore, the porphysome formulation can be easily modified via the liposomal structure to add molecular targeting ligands such as EFGR or folate receptor antibodies in order to further increase tumor-specific accumulation to provide more intense tumor fluorescence and more efficient local ablation (26), as well as enabling personalized lung cancer treatment. The liposomal nanostructure of porphysomes also provides the capability to carry therapeutic and imaging agents, either in the lipid bilayer or in the core, for combinational therapies.

In conclusion, the multifunctional porphysome nanoparticles enabled image-guided focal PTT and improved the specificity and efficiency of PTT compared to laser irradiation alone. The present method is minimally invasive and it can be repeated if required. Porphysome-enhanced transbronchial PTT may provide a new option for a minimally-invasive endoscopic local therapy for the treatment of peripheral lung cancer. We expect that this newly developed platform could be rapidly translated into a novel, curative and safe treatment modality for early-stage lung cancer patients. In addition, this image-guided focal PTT may serve as a model for extension into other localized tumor sites that are amenable to endoscopic intervention.

Supplementary Material

Refer to Web version on PubMed Central for supplementary material.

Acknowledgments

The authors are thankful for the funding from the Canadian Institutes of Health Research (RMF111823 and MOP119597), Ontario Institute for Cancer Research (ZHENG G - OICR – SIP), Natural Sciences and Engineering Research Council of Canada (NSERC-386613-10/UT#489078), Canada Foundation for Innovation (CFI #21765), Joey and Toby Tanenbaum/Brazilian Ball Chair in Prostate Cancer Research, and Princess Margaret Cancer Foundation. We also would like to thank the support from Olympus Medical Systems Inc, Japan, for the development the prototype bronchoscope instrument.

Author Manuscript Author Manuscript Author Manuscript Author Manuscript

C.S.J., H.W., T.A., P.Z.M., B.C.W., G.Z. and K.Y conceived the project and planned the experiment. T.A. and P.Z.M. developed the prototype bronchoscope instrument with Olympus Medical Systems Inc, Japan. H.W., T.A., H.H., K.H., T.N. and T.K. set up animal models. C.S.J. synthesized and characterized porphysomes, carried out the *ex vivo* fluorescence imaging, biodistribution studies and dosimetry studies. C.S.J., H.W., T.A., P.Z.M, H.H., K.H., T.N. and T.K. conducted the *in vivo* bronchoscopy and focal PTT of rabbit lung tumors. T.A. and H.W. prepared the histology slides, and D.W. assisted the histology analysis. C.S.J. and H.W. interpreted the data and wrote the manuscript. P.Z.M., S.K., B.C.W, G.Z., and K.Y contributed in the manuscript editing.

Funding: Canadian Institutes of Health Research (RMF111823 and MOP119597), Ontario Institute for Cancer Research (ZHENG G - OICR – SIP), Natural Sciences and Engineering Research Council of Canada (NSERC-386613-10/UT#489078), Canada Foundation for Innovation (CFI #21765), Joey and Toby Tanenbaum/ Brazilian Ball Chair in Prostate Cancer Research, and Princess Margaret Cancer Foundation.

References

1. Aberle DR, Adams AM, Berg CD, Black WC, Clapp JD, Fagerstrom RM, et al. Reduced lung-cancer mortality with low-dose computed tomographic screening. N Engl J Med. 2011; 365:395–409. [PubMed: 21714641]
2. Timmerman R, Paulus R, Galvin J, Michalski J, Straube W, Bradley J, et al. Stereotactic body radiation therapy for inoperable early stage lung cancer. JAMA. 2010; 303:1070–6. [PubMed: 20233825]
3. Ricardi U, Filippi AR, Guarneri A, Giglioli FR, Ciammella P, Franco P, et al. Stereotactic body radiation therapy for early stage non-small cell lung cancer: results of a prospective trial. Lung Cancer. 2010; 68:72–7. [PubMed: 19556022]
4. Crabtree TD, Puri V, Robinson C, Bradley J, Broderick S, Patterson GA, et al. Analysis of first recurrence and survival in patients with stage I non-small cell lung cancer treated with surgical resection or stereotactic radiation therapy. J Thorac Cardiovasc Surg. 2014; 147:1183–91. discussion 91-2. [PubMed: 24507980]
5. Lagerwaard FJ, Verstegen NE, Haasbeek CJ, Slotman BJ, Paul MA, Smit EF, et al. Outcomes of stereotactic ablative radiotherapy in patients with potentially operable stage I non-small cell lung cancer. Int J Radiat Oncol Biol Phys. 2012; 83:348–53. [PubMed: 22104360]
6. Onishi H, Shirato H, Nagata Y, Hiraoka M, Fujino M, Gomi K, et al. Stereotactic body radiotherapy (SBRT) for operable stage I non-small-cell lung cancer: can SBRT be comparable to surgery? Int J Radiat Oncol Biol Phys. 2011; 81:1352–8. [PubMed: 20638194]
7. Shibamoto Y, Hashizume C, Baba F, Ayakawa S, Manabe Y, Nagai A, et al. Stereotactic body radiotherapy using a radiobiology-based regimen for stage I nonsmall cell lung cancer: a multicenter study. Cancer. 2012; 118:2078–84. [PubMed: 22009495]
8. Grills IS, Mangona VS, Welsh R, Chmielewski G, McInerney E, Martin S, et al. Outcomes after stereotactic lung radiotherapy or wedge resection for stage I non-small-cell lung cancer. J Clin Oncol. 2010; 28:928–35. [PubMed: 20065181]
9. Crabtree TD, Denlinger CE, Meyers BF, El Naqa I, Zoole J, Krupnick AS, et al. Stereotactic body radiation therapy versus surgical resection for stage I non-small cell lung cancer. J Thorac Cardiovasc Surg. 2010; 140:377–86. [PubMed: 20400121]
10. Hiraki T, Gobara H, Mimura H, Matsui Y, Toyooka S, Kanazawa S. Percutaneous radiofrequency ablation of clinical stage I non-small cell lung cancer. J Thorac Cardiovasc Surg. 2011; 142:24–30. [PubMed: 21529847]
11. Lanuti M, Sharma A, Willers H, Digumarthy SR, Mathisen DJ, Shepard JA. Radiofrequency ablation for stage I non-small cell lung cancer: management of locoregional recurrence. Ann Thorac Surg. 2012; 93:921–7. discussion 7-88. [PubMed: 22296982]
12. Ambrogi MC, Fanucchi O, Cioni R, Dini P, De Liperi A, Cappelli C, et al. Long-term results of radiofrequency ablation treatment of stage I non-small cell lung cancer: a prospective intention-to-treat study. J Thorac Oncol. 2011; 6:2044–51. [PubMed: 22052222]
13. Lencioni R, Crocetti L, Cioni R, Suh R, Glenn D, Regge D, et al. Response to radiofrequency ablation of pulmonary tumours: a prospective, intention-to-treat, multicentre clinical trial (the RAPTURE study). Lancet Oncol. 2008; 9:621–8. [PubMed: 18565793]

Author Manuscript Author Manuscript Author Manuscript Author Manuscript

14. Simon CJ, Dupuy DE, DiPetrillo TA, Safran HP, Grieco CA, Ng T, et al. Pulmonary radiofrequency ablation: long-term safety and efficacy in 153 patients. Radiology. 2007; 243:268–75. [PubMed: 17392258]
15. Bolliger CT, Sutedja TG, Strausz J, Freitag L. Therapeutic bronchoscopy with immediate effect: laser, electrocautery, argon plasma coagulation and stents. Eur Respir J. 2006; 27:1258–71. [PubMed: 16772389]
16. Simone CB 2nd, Friedberg JS, Glatstein E, Stevenson JP, Sterman DH, Hahn SM, et al. Photodynamic therapy for the treatment of non-small cell lung cancer. J Thorac Dis. 2012; 4:63–75. [PubMed: 22295169]
17. Yang X, Ye X, Zheng A, Huang G, Ni X, Wang J, et al. Percutaneous microwave ablation of stage I medically inoperable non-small cell lung cancer: Clinical evaluation of 47 cases. J Surg Oncol. 2014; 110:758–63. [PubMed: 24965604]
18. Niu L, Xu K, Mu F. Cryosurgery for lung cancer. J Thorac Dis. 2012; 4:408–19. [PubMed: 22934144]
19. Okunaka T, Kato H, Tsutsui H, Ishizumi T, Ichinose S, Kuroiwa Y. Photodynamic therapy for peripheral lung cancer. Lung Cancer. 2004; 43:77–82. [PubMed: 14698541]
20. Henderson BW, Fingar VH. Relationship of tumor hypoxia and response to photodynamic treatment in an experimental mouse tumor. Cancer Res. 1987; 47:3110–4. [PubMed: 3581062]
21. Sitnik TM, Hampton JA, Henderson BW. Reduction of tumour oxygenation during and after photodynamic therapy in vivo: effects of fluence rate. Br J Cancer. 1998; 77:1386–94. [PubMed: 9652753]
22. Jin CS, Lovell JF, Chen J, Zheng G. Ablation of hypoxic tumors with dose-equivalent photothermal, but not photodynamic, therapy using a nanostructured porphyrin assembly. ACS Nano. 2013; 7:2541–50. [PubMed: 23394589]
23. Boulnois J-L. Photophysical processes in recent medical laser developments: A review. Lasers Med Sci. 1986; 1:47–66.
24. Nikfarjam M, Muralidharan V, Christophi C. Mechanisms of focal heat destruction of liver tumors. J Surg Res. 2005; 127:208–23. [PubMed: 16083756]
25. Lovell JF, Jin CS, Huynh E, Jin H, Kim C, Rubinstein JL, et al. Porphysome nanovesicles generated by porphyrin bilayers for use as multimodal biophotonic contrast agents. Nat Mater. 2011; 10:324–32. [PubMed: 21423187]
26. Jin CS, Cui L, Wang F, Chen J, Zheng G. Targeting-Triggered Porphysome Nanostructure Disruption for Activatable Photodynamic Therapy. Adv Healthc Mater. 2014; 3:1240–9. [PubMed: 24464930]
27. Maeda H, Nakamura H, Fang J. The EPR effect for macromolecular drug delivery to solid tumors: Improvement of tumor uptake, lowering of systemic toxicity, and distinct tumor imaging in vivo. Adv Drug Deliv Rev. 2013; 65:71–9. [PubMed: 23088862]
28. Huynh E, Zheng G. Porphysome nanotechnology: A paradigm shift in lipid-based supramolecular structures. Nano Today. 2014; 9:212–22.
29. Jin CS, Lovell JF, Zheng G. One minute, sub-one-watt photothermal tumor ablation using porphysomes, intrinsic multifunctional nanovesicles. J Vis Exp. 2013; (79):e50536. [PubMed: 24084712]
30. Muhanna N, Jin CS, Huynh E, Chan H, Qiu Y, Jiang W, et al. Phototheranostic Porphyrin Nanoparticles Enable Visualization and Targeted Treatment of Head and Neck Cancer in Clinically Relevant Models. Theranostics. 2015; 5:1428–43. [PubMed: 26681987]
31. Nakajima T, Anayama T, Matsuda Y, Hwang DM, McVeigh PZ, Wilson BC, et al. Orthotopic lung cancer murine model by nonoperative transbronchial approach. Ann Thorac Surg. 2014; 97:1771–5. [PubMed: 24792261]
32. Anayama T, Nakajima T, Dunne M, Zheng J, Allen C, Driscoll B, et al. A novel minimally invasive technique to create a rabbit VX2 lung tumor model for nano-sized image contrast and interventional studies. PLoS One. 2013; 8:e67355. [PubMed: 23840673]
33. Choi MJ, Guntur SR, Lee KI, Paeng DG, Coleman A. A tissue mimicking polyacrylamide hydrogel phantom for visualizing thermal lesions generated by high intensity focused ultrasound. Ultrasound Med Biol. 2013; 39:439–48. [PubMed: 23312531]

Author Manuscript Author Manuscript Author Manuscript Author Manuscript

34. Cobley CM, Au L, Chen J, Xia Y. Targeting gold nanocages to cancer cells for photothermal destruction and drug delivery. Expert Opin Drug Deliv. 2010; 7:577–87. [PubMed: 20345327]
35. Neumann RA, Knobler RM, Pieczkowski F, Gebhart W. Enzyme histochemical analysis of cell viability after argon laser-induced coagulation necrosis of the skin. J Am Acad Dermatol. 1991; 25:991–8. [PubMed: 1810998]
36. Awad MM, Devgan L, Kamel IR, Torbensen M, Choti MA. Microwave ablation in a hepatic porcine model: correlation of CT and histopathologic findings. HPB (Oxford). 2007; 9:357–62. [PubMed: 18345319]
37. Liu TW, Macdonald TD, Jin CS, Gold JM, Bristow RG, Wilson BC, et al. Inherently Multimodal Nanoparticle-Driven Tracking and Real-Time Delineation of Orthotopic Prostate Tumors and Micrometastases. ACS Nano. 2013; 7:4221–32. [PubMed: 23544841]
38. Hirohashi K, Anayama T, Wada H, Nakajima T, Kato T, Keshavjee S, et al. Photothermal ablation of human lung cancer by low-power near-infrared laser and topical injection of indocyanine green. Journal of bronchology & interventional pulmonology. 2015; 22:99–106. [PubMed: 25887004]
39. Yuan B, Chen N, Zhu Q. Emission and absorption properties of indocyanine green in Intralipid solution. Journal of biomedical optics. 2004; 9:497–503. [PubMed: 15189087]
40. Lu DS, Raman SS, Vodopich DJ, Wang M, Sayre J, Lassman C. Effect of vessel size on creation of hepatic radiofrequency lesions in pigs: assessment of the “heat sink” effect. AJR Am J Roentgenol. 2002; 178:47–51. [PubMed: 11756085]
41. Lu DS, Raman SS, Limanond P, Aziz D, Economou J, Busuttil R, et al. Influence of large peritumoral vessels on outcome of radiofrequency ablation of liver tumors. J Vasc Interv Radiol. 2003; 14:1267–74. [PubMed: 14551273]
42. Oshima F, Yamakado K, Akeboshi M, Takaki H, Nakatsuka A, Makita M, et al. Lung radiofrequency ablation with and without bronchial occlusion: experimental study in porcine lungs. J Vasc Interv Radiol. 2004; 15:1451–6. [PubMed: 15590804]
43. Lindner U, Weersink RA, Haider MA, Gertner MR, Davidson SR, Atri M, et al. Image guided photothermal focal therapy for localized prostate cancer: phase I trial. J Urol. 2009; 182:1371–7. [PubMed: 19683262]
44. Rendon A, et al. Towards conformal light delivery using tailored cylindrical diffusers: attainable light dose distributions. Phys Med Biol. 2006; 51:5967–75. [PubMed: 17110763]
45. Liu TW, MacDonald TD, Shi J, Wilson BC, Zheng G. Intrinsically Copper-64-Labeled Organic Nanoparticles as Radiotracers. Angew Chem Int Ed. 2012; 51:13128–31.
46. Muhanna N, MacDonald TD, Chan H, Jin CS, Burgess L, Cui L, et al. Multimodal Nanoparticle for Primary Tumor Delineation and Lymphatic Metastasis Mapping in a Head-and-Neck Cancer Rabbit Model. Adv Healthc Mater. 2015; 4:2164–9.
47. MacDonald TD, Liu TW, Zheng G. An MRI-Sensitive, Non-Photobleachable Porphysome Photothermal Agent. Angew Chem Int Ed Engl. 2014; (53):6956–9. [PubMed: 24840234]

Author Manuscript Author Manuscript Author Manuscript Author Manuscript

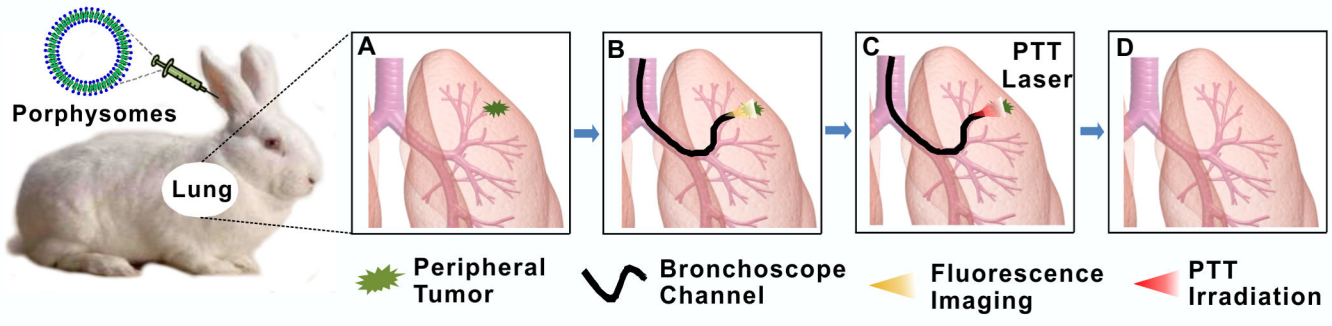

Figure 1.

The concept of ultra-minimally invasive, multi-modal, fluorescence-guided transbronchial photothermal therapy of early-stage peripheral lung cancer: **(A)** porphysomes are administered intravenously and accumulate in the tumor; **(B)** bronchoscopic fluorescence visualization of dissociated porphysomes in the target tumor at 48 h post-injection; **(C)** localized transbronchial photothermal irradiation; **(D)** tumor ablated by ultra minimally invasive PTT.

Author Manuscript Author Manuscript Author Manuscript Author Manuscript

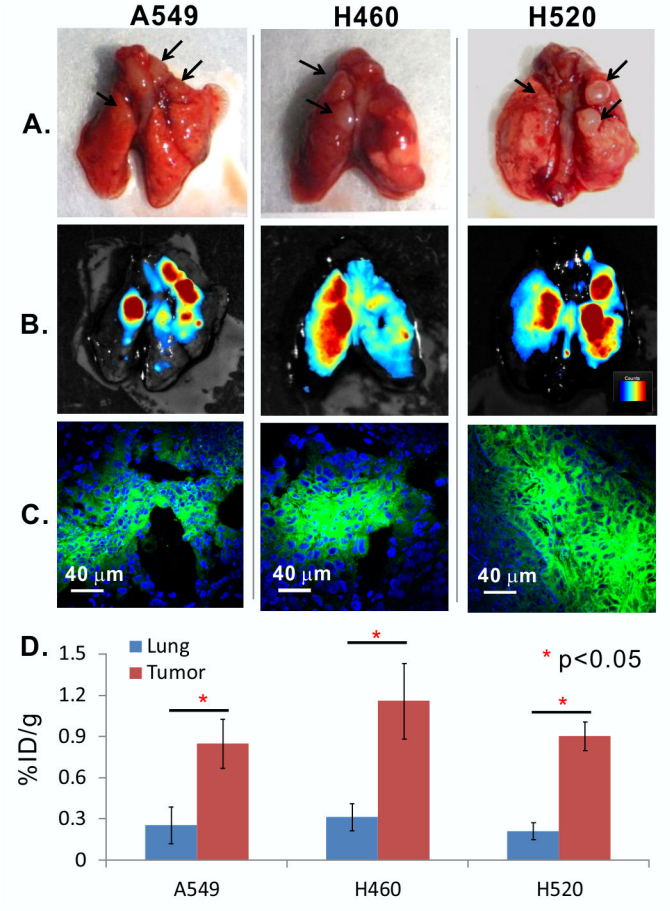

Figure 2.

Porphysome accumulation at 48h post IV injection in human lung cancer xenografts in nude mice, including three subtypes: A549 adenocarcinoma, H460 large cell carcinoma and H520 squamous cell carcinoma. **(A)** white-light images of excised tumor-bearing lung (scale bar 5 mm); **(B)** corresponding fluorescence images with false-color coding for intensity (70-700 Maestro™ units)(scale bar 5 mm); **(C)** confocal microscopy images of tumor showing both porphyrin (green) and DAPI (blue) distributions (scale bar 40 μm); **(D)** porphysome accumulation in tumor and normal lung and each tumor subtype (n=5): mean ± S.D. * represents $p<0.05$.

Author Manuscript Author Manuscript Author Manuscript Author Manuscript

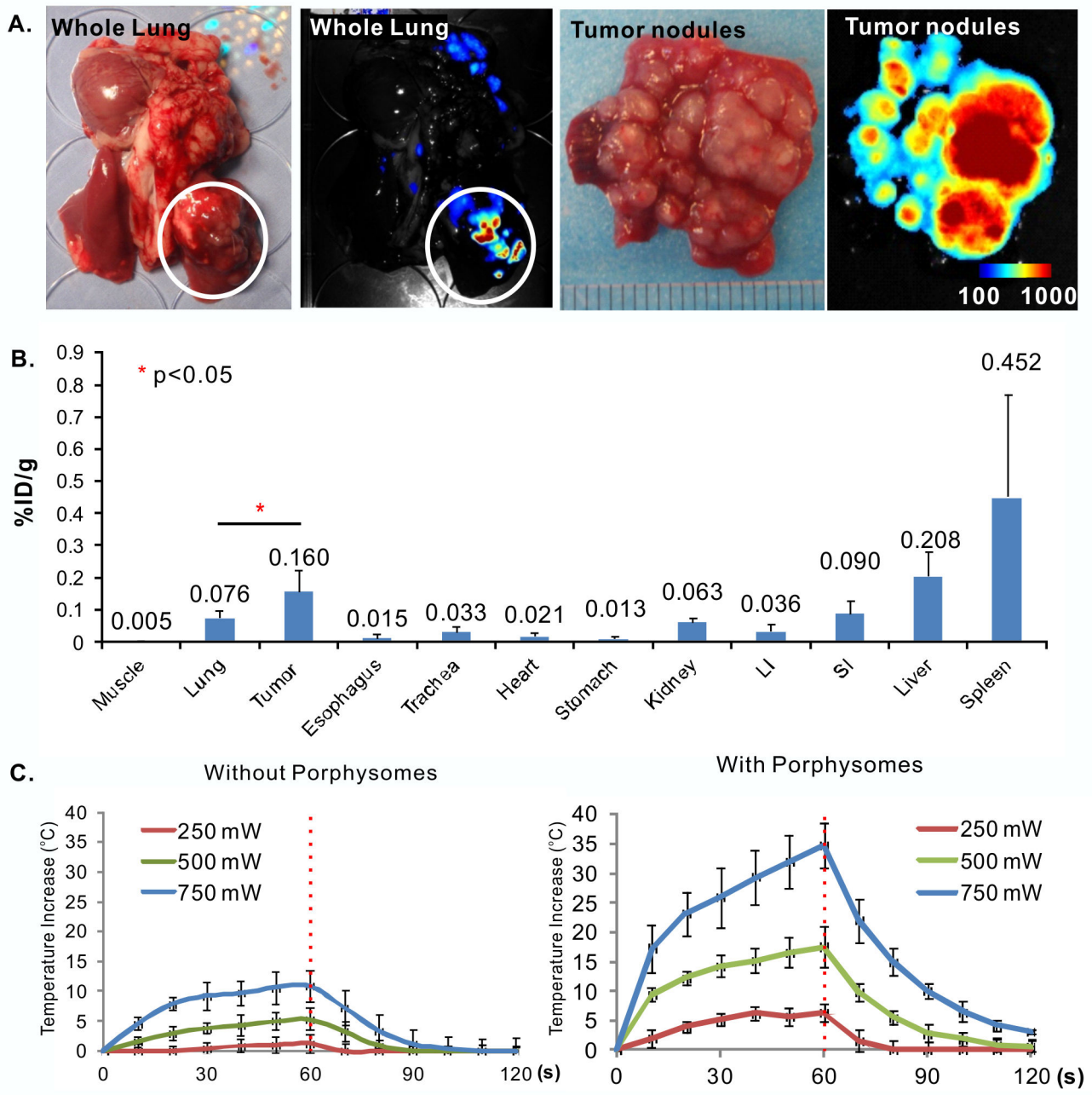

Figure 3.

Porphysome accumulation in VX2 tumor in rabbit lung. **(A)** *ex vivo* white-light and fluorescence images of intact lung and tumor cross-sections (Scale bar: 100-1000 Maestro™ unit); **(B)** biodistribution of porphysomes in organs at 48 h post IV injection, n=4 for means ± S.D.; **(C)** time curves of mean temperature change of tumor during and after *ex vivo* PTT at different laser powers with and without porphysomes (n=3 in each group). Laser was turned off at 60s and indicated by the red dashed line.

Author Manuscript Author Manuscript Author Manuscript Author Manuscript

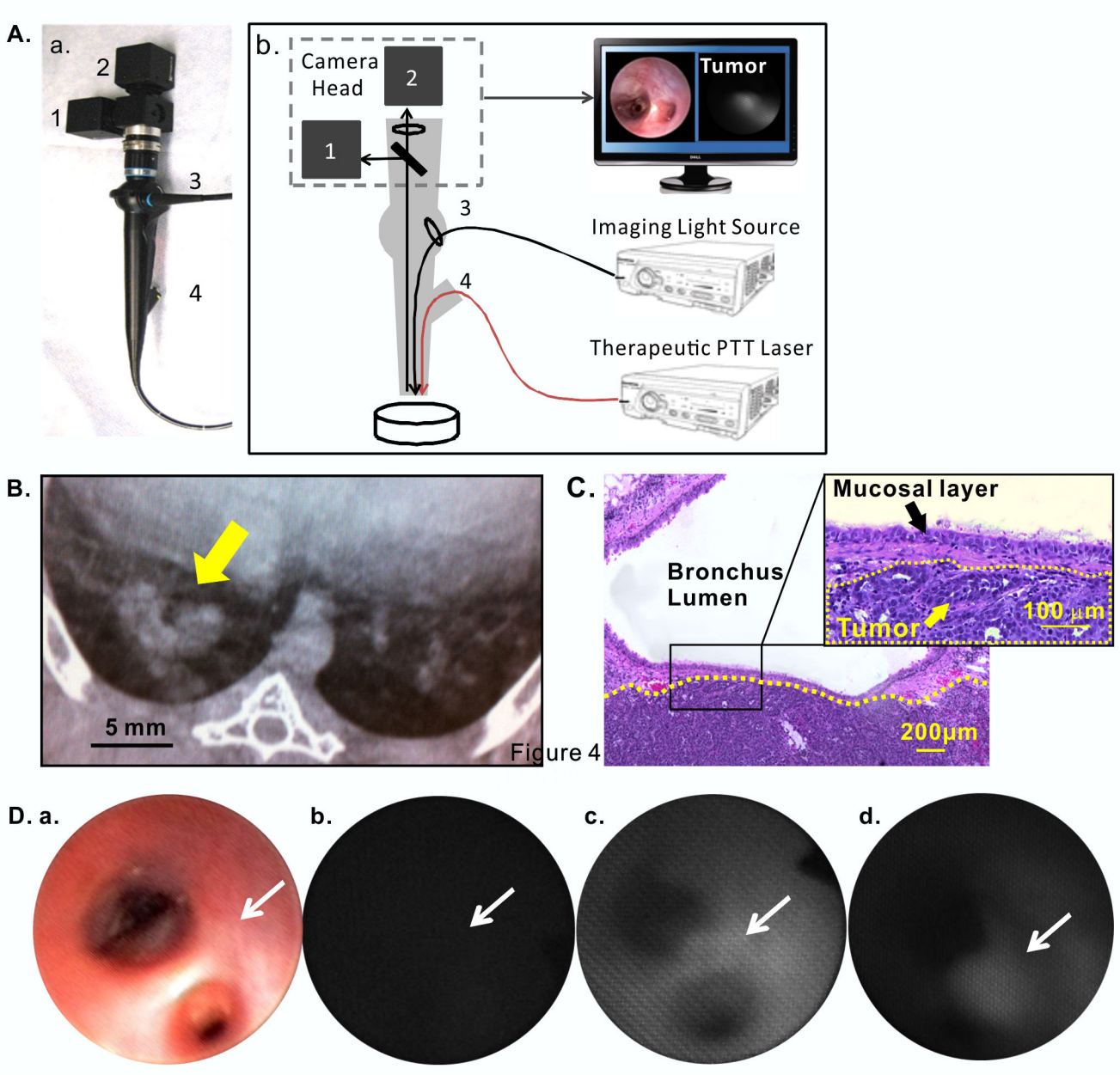

Figure 4.

In vivo fluorescence imaging of VX2 tumor in rabbit lung. **(A) a,** hand-held prototype bronchoscope; **b**, scheme of the components; 1: Color CCD camera for white light imaging; 2: 660 nm notch filter + monochrome CCD camera for fluorescence imaging; 3: endoscopic light source: 660nm laser combined with programmable LED white light source; 4: endoscope accessory channel for 671 nm high power fiber-coupled laser used for PTT therapy; **(B)** CT scan of showing the location of the VX2 tumor mass in the lung (yellow arrow); **(C)** H&E staining, indicating VX2 tumor (the area below the yellow dash line) in the lung parenchyma located in the sub-mucosal layer without extension to the endobronchial lumen; **(D)** *in vivo* bright-field (a) and corresponding fluorescence bronchoscopic images

captured at: (b) pre-injection, (c) 24 h and (d) 48 h post-IV porphysome injection: white arrow indicates the location of tumor.

Author Manuscript Author Manuscript Author Manuscript Author Manuscript

Author Manuscript Author Manuscript Author Manuscript Author Manuscript

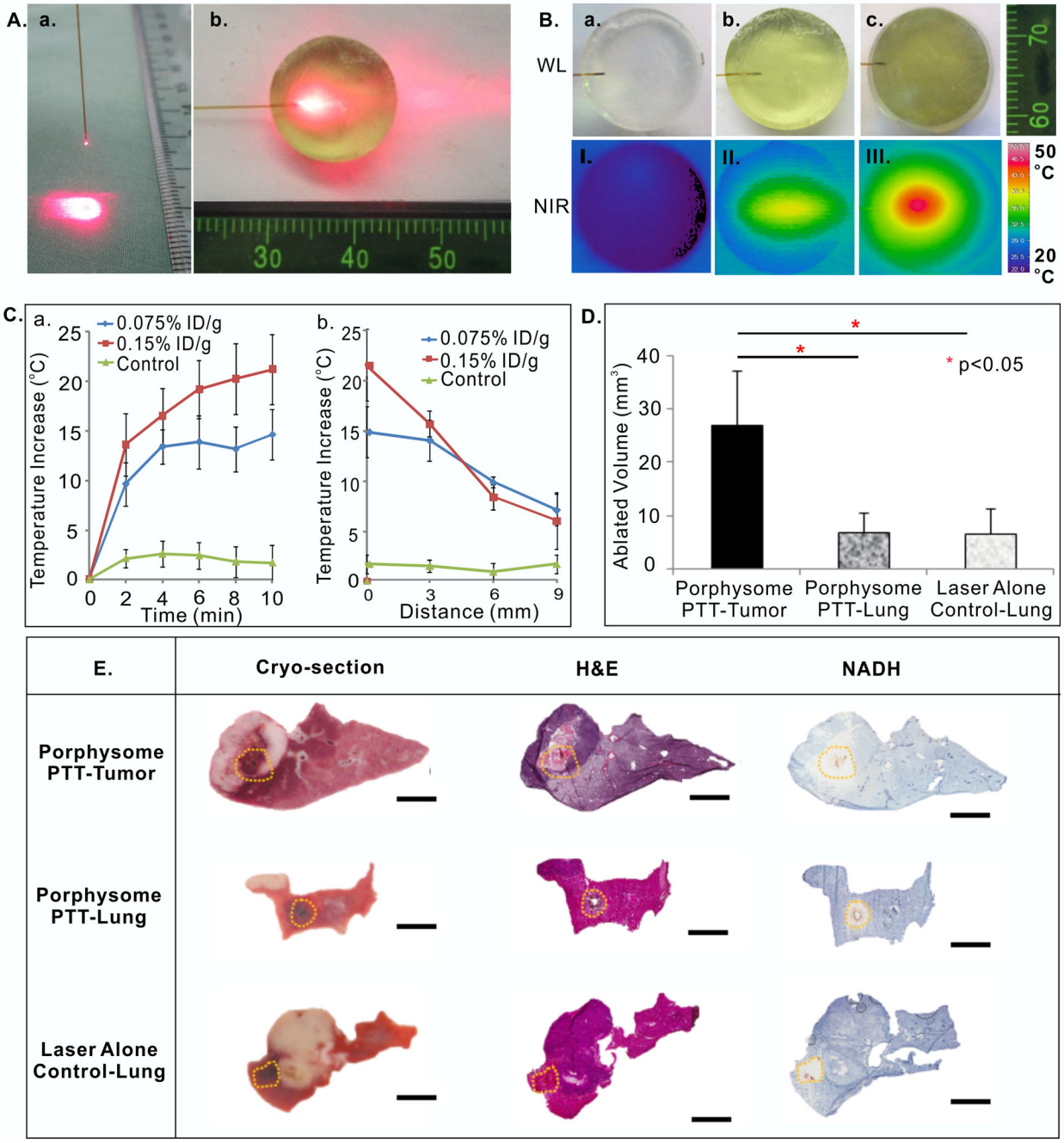

Figure 5.

In vivo transbronchial porphysome-enhanced PTT in the rabbit model using a straight-cut fiber at 250 mW. **(A)** straight-cut fiber (a) and phantom set-up (b); **(B)** White light (WL) and near infrared thermal images (NIR) of phantoms upon 250 mW laser irradiation at different porphysome concentrations (a, no porphysomes control; b, 0.076%ID/g; c, 0.16% ID/g); **(C)** temperature change in phantoms with different porphysome concentrations for laser power of 250 mW; a, maximum temperature increase during irradiation (by minute) and b, maximum temperature increase as a function of axial distance at the forward direction from

Author Manuscript Author Manuscript Author Manuscript Author Manuscript

the fiber tip following 10 min irradiation; **(D)** *in vivo* ablated tumor volume (mean ± S.D.: n=4,5,4); **(E)** corresponding gross sections of histology analysis of ablation zones in porphysome-containing tumor, porphysome-containing normal lung and in uninjected control lung. The orange dotted line indicates the ablation boundary identified based on NADH stains. Scale bars: 4 mm. * represents $p<0.05$.

Author Manuscript Author Manuscript Author Manuscript Author Manuscript

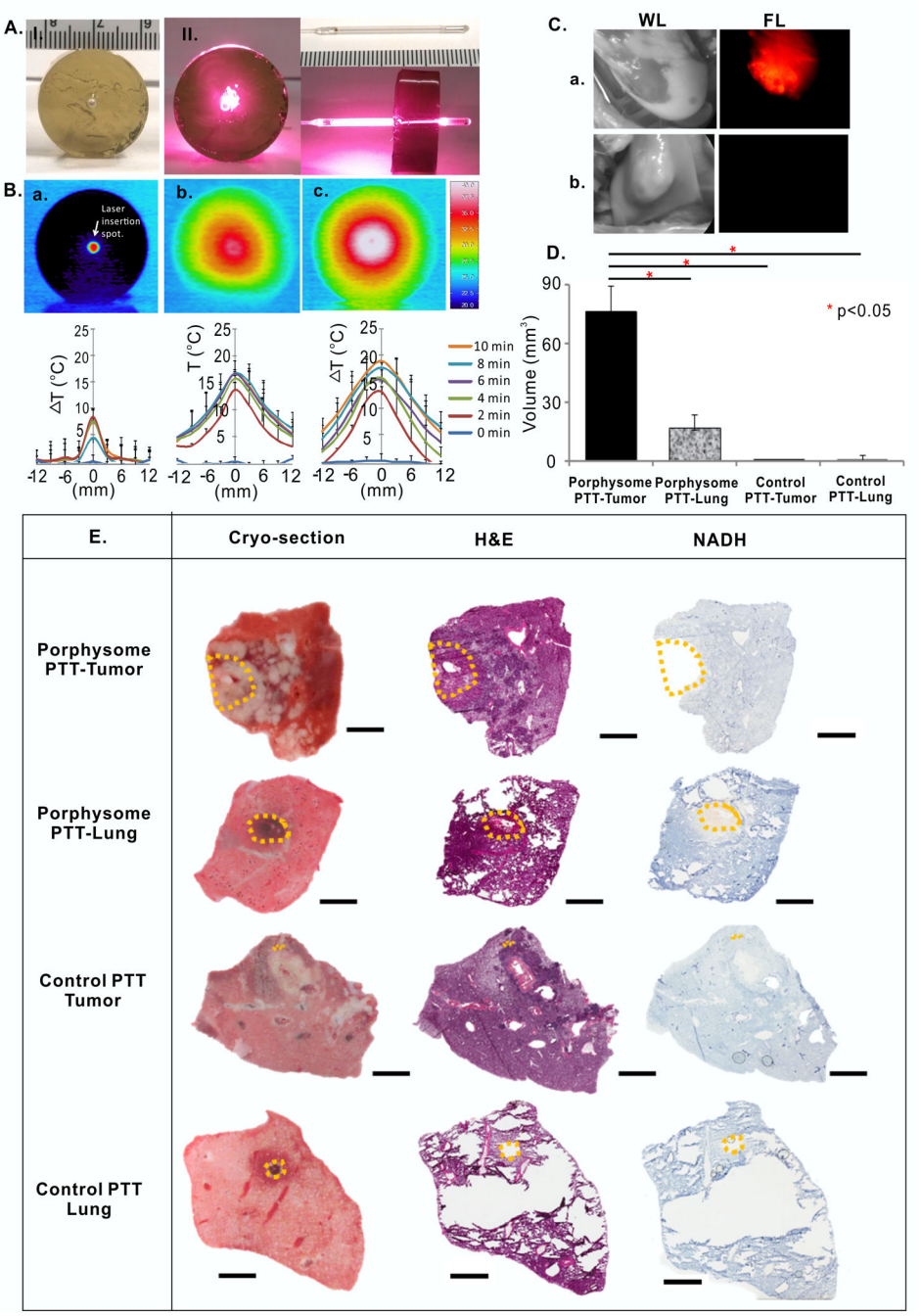

Figure 6.

In vivo transpleural porphysome-enabled fluorescence localization and PTT in the rabbit model using a diffuser fiber at 500 mW/cm. **(A)** phantom (a) and cylindrical diffuser laser set-up (b); **(B)** Dosimetry study using phantoms containing different porphysome concentrations (a, no porphysome control; b, 0.076 %ID/g; c, 0.16 %ID/g) at 500 mW/cm power, and corresponding temperature increases along the distance away from the fiber (mm); **(C)** white light (WL) and fluorescence (FL) images of lung tumor with porphysome injection (a) were compared to the control rabbit without porphysome injection (b); **(D)** *in*

Author Manuscript Author Manuscript Author Manuscript Author Manuscript

vivo ablated tumor volume (mean ± S.D., n=3,4,4,3) at 500 mW/cm power; **(E)** corresponding gross sections of histology analysis to evaluate the ablated area in porphysome containing tumor, porphysome containing lung, control tumor without porphysome injection, and control lung without porphysome injection. The orange dotted line indicates the ablation boundary identified based on NADH stains. Scale bars: 4 mm. * represents $p<0.05$.